ARTICLE

Huge Tunneling Magnetoresistance in Magnetic Tunnel Junction with Heusler Alloy Co_2MnSi Electrodes

Yu-jie Hu[a], Jing Huang[b*], Jia-ning Wang[a], Qun-xiang Li[a*]

a. Department of Chemical Physics & Hefei National Laboratory for Physical Sciences at the Microscale, University of Science and Technology of China, Hefei 230026, China
b. School of Materials and Chemical Engineering, Anhui Jianzhu University, Hefei 230601, China

(Dated: Received on September 24, 2020; Accepted on October 22, 2020)

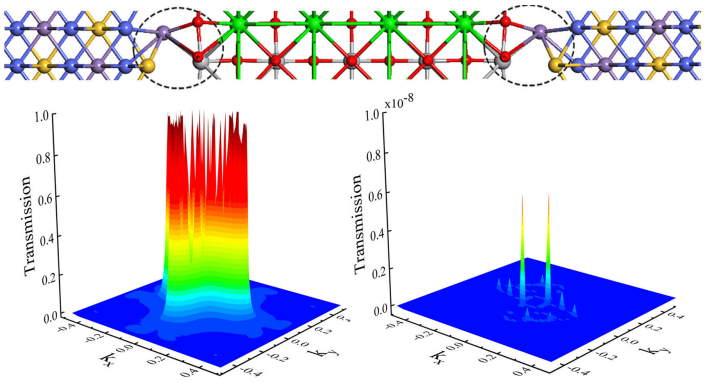

Magnetic tunnel junction with a large tunneling magnetoresistance has attracted great attention due to its importance in the spintronics applications. By performing extensive density functional theory calculations combined with the nonequilibrium Green's function method, we explore the spin-dependent transport properties of a magnetic tunnel junction, in which a non-polar $SrTiO_3$ barrier layer is sandwiched between two Heusler alloy Co_2MnSi electrodes. Theoretical results clearly reveal that the near perfect spin-filtering effect appears in the parallel magnetization configuration. The transmission coefficient in the parallel magnetization configuration at the Fermi level is several orders of magnitude larger than that in the antiparallel magnetization configuration, resulting in a huge tunneling magnetoresistance (*i.e.* $>10^6$), which originates from the coherent spin-polarized tunneling, due to the half-metallic nature of Co_2MnSi electrodes and the significant spin-polarization of the interfacial Ti 3d orbital.

Key words: Magnetic tunnel junction, Spin-dependent transport, First-principles, Tunneling magnetoresistance

I. INTRODUCTION

Magnetic tunnel junction (MTJ), in which a non-polar band insulator is sandwiched between two ferromagnetic electrodes, has attracted great attention for years since it plays an important role for applications in spintronics. Generally, the tunneling resistance varies as a function of the relative magnetic configuration of the electrodes, resulting in an effect called tunneling magnetoresistance (TMR) [1]. The TMR effect is of great importance in spintronics, such as magnetic sensor and magnetic random access memory [2, 3]. Previous experimental and theoretical investigations mainly focused on magnetic metals (*i.e.* Fe, Co, Ni) and magnetic alloys like CoFeB as electrodes in various magnetic tunnel junctions [4–10]. Note that one central issue in MTJs is how to efficiently inject spin polarized electrons from the ferromagnetic electrodes into the sandwiched insulating layer. The low spin polarizability of ferromagnetic metal will lead to low spin injection efficiency. Therefore, one effective way to improve the performance of TMJs is using the half-metallic ferromagnets (HMFs), *i.e.* Fe_3O_4 [11] and $La_{0.7}Sr_{0.3}MnO_3$ [12], as electrodes [13–15], since the HMFs carry cur-

*Authors to whom correspondence should be addressed. E-mail: jhuang@ustc.edu.cn, liqun@ustc.edu.cn

 ©2021 Chinese Physical Society

rent in only one spin channel, leading to complete spin polarization at the Fermi level [16], greatly enhancing the spin injection efficiency. For example, in experiments, the MTJ with manganite $La_{0.7}Sr_{0.3}MnO_3$ electrodes and $SrTiO_3$ barrier layer has achieved a large TMR ratio of 1800% at low temperature [17].

As one kind of half-metallic materials, Heusler compounds (especially, Co-based full-Heusler alloys) have been widely used as electrodes in MTJs, which display attractive performance, *i.e.* the high TMR effect of several hundred percent [18–20]. Due to the high Curie temperature (∼985 K) above room temperature and the nearly perfect spin polarized around the Fermi level [21], half-metallic Co-based full-Heusler alloys hold the most potential for applications in spintronics devices, and they have been widely conducted on TMR measurements for various MTJs with AlO_x or MgO barrier layer and Co-based Heusler alloys, such as, $Co_2Fe(Al_{0.5}Si_{0.5})$, Co_2MnSi, Co_2MnAl, and so on [22–26].

Recently, Rout *et al.* have successfully grown $L2_1$-type Co_2MSi (M=Mn and Fe) on a variety of semiconductors and oxide dielectrics (*i.e.* $SrTiO_3$) and measured two-dimensional electron-gas-like charge transport at the interface between a Heusler alloy Co_2MSi (M=Mn or Fe) and $SrTiO_3$ in their experiments [27]. Nazir *et al.* recently performed spin-polarized density functional theory calculations on the structural and charge transfer at the TiO_2 terminated interfaces between the magnetic Heusler alloys Co_2MSi (M=Ti, V, Cr, Mn, and Fe) and the non-polar band insulator $SrTiO_3$ (barrier layer) [28]. However, theoretical spin-dependent transport investigation of these corresponding MTJs is lacking so far.

In this work, we explore the spin-dependent transport properties of $Co_2MnSi/SrTiO_3/Co_2MnSi$ MTJs with different interfaces by performing extensive density functional theory (DFT) calculations combined with the nonequilibrium Green's function (NEGF) technique. According to the calculated zero-bias transmission spectra of the MTJ with the MnSi-TiO_2 interface, we find that the transmission coefficient at the Fermi level in the parallel magnetization configuration (PC) is several orders of magnitude larger than in the antiparallel magnetization configuration (APC), resulting in a huge TMR (*i.e.* $>10^6$), which is significantly larger than previous reports for MTJs with Co_2MnSi electrode or $SrTiO_3$ barrier layer [14, 26, 29, 30]. Moreover, the nearly perfect spin-filtering effect is observed in the examined MTJ in the PC. Through analysing the projected density of states (DOS) of MTJ, the partial DOS of the atoms in the interface, and the in-plane wave vector dependence of transmission spectra, we find that the huge TMR originates from the coherent spin-polarized tunneling, due to the half-metallic nature of Heusler alloy Co_2MnSi electrodes and the significant spin-polarization of the interfacial Ti 3d orbital.

II. COMPUTATIONAL METHODS

The geometric optimizations and electronic structure calculations in this work are carried out by using DFT within Perdew-Burke-Ernzerh (PBE) of the generalized gradient approximation (GGA) exchange correlation functional implemented in the Vienna *ab initio* simulation package (VASP) [31–33]. We adopt a plane-wave basis adjusted by expanding the Kohn-Sham orbitals with a 520 eV kinetic energy cutoff. A k-mesh of 10×10×1 is used, and the Hellmann-Feynman forces acting on each atom are less than 0.02 eV/Å for geometric optimization.

The spin-dependent transport properties of these examined MTJs are explored by performing DFT calculations combined with the NEGF technique, implemented in the ATK package [34, 35]. In our calculations, the GGA in the PBE form is used to describe the exchange and correlation energy, the double-zeta polarized basis sets are adopted for all atoms, a Monkhorst-Pack k-mesh of 10×10×100 is used to converge the density matrix, a 100×100 $k_\parallel$ meshes is adopted to calculate transmission coefficient, and a cutoff energy is set to be 160 Ry for the real-space grid. The spin-dependent conductance per unit cell is given by the Landauer-Büttiker formula,

$$G_\sigma = \frac{e^2}{h}\sum_{k_\parallel,j} T^+(k_\parallel, j) \tag{1}$$

here, σ stands for the spin-up (↑) and spin-down (↓) channels, j represents the Bloch state for a given value of $k_\parallel$=k_x+k_y, and $T^+(k_\parallel, j)$ represents the transmission probability of an electron at the Fermi level with spin (σ) and the Bloch wave vector ($k_\parallel$). Then, the TMR ratio at zero bias voltage is defined as

$$\mathrm{TMR} = \frac{G_{\mathrm{PC}} - G_{\mathrm{APC}}}{G_{\mathrm{APC}}} \times 100\% \tag{2}$$

where, G_{PC} and G_{APC} stand for the conductance of

DOI:10.1063/1674-0068/cjcp2009170 ©2021 Chinese Physical Society

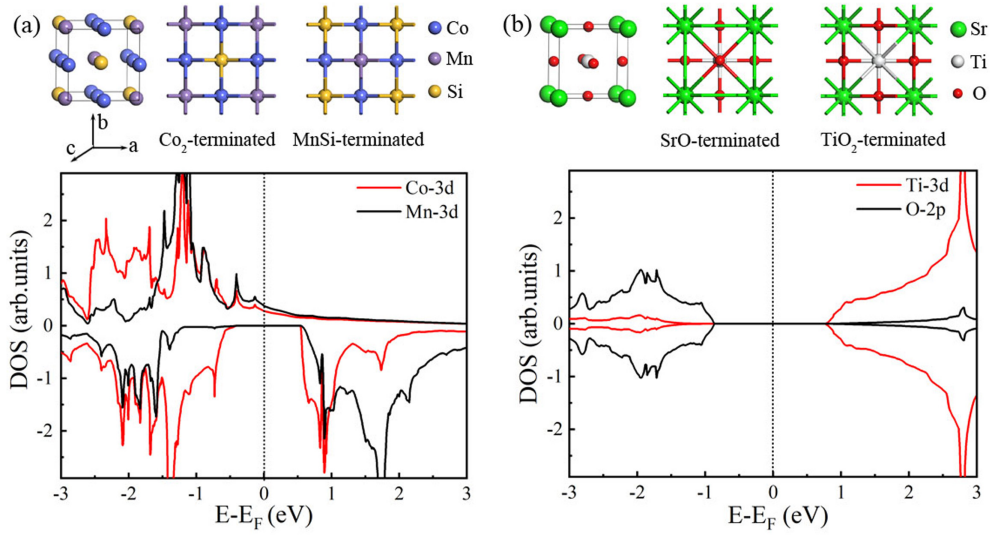

FIG. 1 (a) Atomic lattice of bulk Co_2MnSi, and the top view of Co_2-terminated and MnSi-terminated surfaces. (b) Atomic lattice of bulk $SrTiO_3$, and the top view of SrO-terminated and TiO_2-terminated surfaces. (c) The partial DOS of Co 3d and Mn 3d orbitals in bulk Co_2MnSi, labeled with the red and black lines, respectively. (d) The partial DOS of Ti 3d (red line) and O 2p (black line) orbitals in bulk $SrTiO_3$.

magnetic tunnel junction in the parallel magnetization configuration, and antiparallel magnetization configuration, respectively.

III. RESULTS AND DISCUSSION

Before exploring spin-dependent transport properties of $Co_2MnSi/SrTiO_3/Co_2MnSi$ MTJs, we firstly examine the geometric and electronic properties of bulk Co_2MnSi and $SrTiO_3$. FIG. 1(a) shows the optimized geometric structure of bulk Co_2MnSi. The optimized lattice constant is about 3.974 Å, corresponding to $a_0/\sqrt{2}$ of cubic $L2_1$-type Co_2MnSi. The spin-polarized parital DOS of Co 3d and Mn 3d orbitals of bulk Co_2MnSi are plotted in FIG. 1(c) with the red and black lines, respectively. Clearly, one can observe half-metallicity for bulk Co_2MnSi. That is to say, the spin-up channel, contributed by the Co 3d and Mn 3d orbitals, is metallic, while the spin-down channel is insulating with a band gap of 0.5 eV. The atomic magnetic moments of Co and Mn atom are predicted to be 1.0 and 3.0 μ_B. While for bulk $SrTiO_3$, as shown in FIG. 1(b), the lattice constant is 3.914 Å. The calculated partial DOS of Ti 3d and O 2p orbitals plotted in FIG. 1(d) show that $SrTiO_3$ is a nonmagnetic semiconductor with a band gap of 1.7 eV, since the spin-up DOS coincides exactly with the spin-down DOS. These structural parameters and electronic structures of bulk Co_2MnSi and $SrTiO_3$ agree well with previous experimental and theoretical reports [36–38].

There are two different terminations for Co_2MnSi and $SrTiO_3$ along c direction (transport direction). Namely, Co_2-terminated and MnSi-terminated for Heusler alloy Co_2MnSi electrode, SrO-terminated and TiO_2-terminated for $SrTiO_3$ barrier layer, are illustrated in FIG. 1 (a) and (b), respectively. Therefore, we construct four possible $Co_2MnSi/SrTiO_3/Co_2MnSi$ MTJs with the MnSi-TiO_2, MnSi-SrO, Co_2-SrO, and Co_2-TiO_2 interfaces, which are named with MTJ1, MTJ2, MTJ3 and MTJ4 for short, respectively. Due to the slight different lattice constants, there is a small in-plane lattice mismatch of 1.5% between Co_2MnSi electrodes and $SrTiO_3$ barrier layer. To find the most energetically stable junction, we calculate the interfacial energy (E_{int}), which is defined as

$$E_{int} = E_{tot} - \sum N_i \mu_i \tag{3}$$

here, E_{tot} stands for the total energy, N_i is the atomic number of each element, and μ_i is the atomic chemical potential. The optimized interfacial distances and the calculated interfacial energies are summarized in Table I. It is clear that MTJ1 is the most stable junction with the MnSi-TiO_2 interface, in which Mn atoms sit on the hollow site of TiO_2 layer with the relaxed vertical distance of 1.8 Å, as shown in FIG. 2(a). This kind of MSi-TiO_2 (M=Fe or Mn) interface has been examined by scanning transmission electron microscopy

DOI:10.1063/1674-0068/cjcp2009170 ©2021 Chinese Physical Society

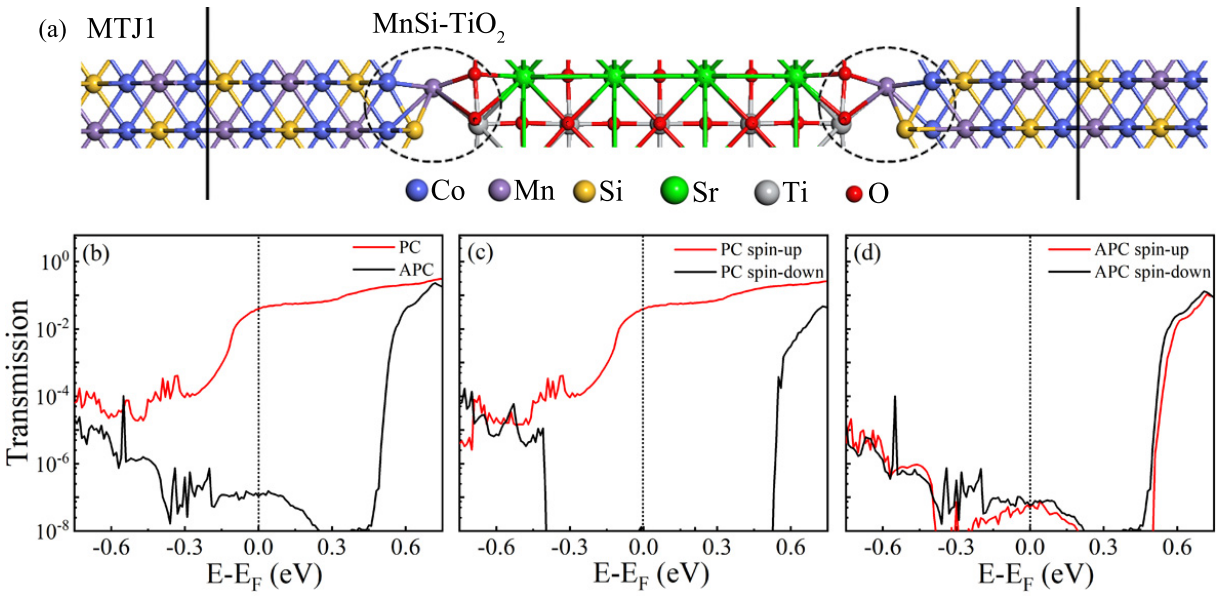

FIG. 2 (a) The optimized atomic structure of MTJ1, in which a $SrTiO_3$ barrier layer (4.5 unitcells) is sandwiched between two Heusler alloy Co_2MnSi electrodes with the MnSi-TiO_2 interface. (b) The zero-bias transmission spectra of MTJ1 in the PC (parallel magnetization configuration) and APC (antiparallel magnetization configuration), labeled with the red and black lines, respectively. The spin-resolved transmission spectra of MTJ1 in (c) PC and (d) APC, here, the blue and black lines stand for the spin-up and spin-down electrons, respectively.

imaging [27]. In our calculations, the proposed MTJ can be divided into three parts: the central scattering region, left and right Co_2MnSi electrodes. The scattering region consists of 9 atomic layers of $SrTiO_3$ and 13 atomic layers of two electrodes. Then, we take MTJ1 as an example to explore the spin-dependent transport properties of $Co_2MnSi/SrTiO_3/Co_2MnSi$ MTJs.

To investigate the spin-dependent transport properties of MTJ1, we calculate their zero-bias transmission spectra and plot them in FIG. 2(b), here, the red and black lines stand for the transmission spectra for the PC and APC, respectively. It is clear that the zero-bias transmission spectra of two magnetization configurations show remarkable different feature. The transmission curve of the PC (red line) is smooth around the Fermi level, and the transmission coefficients are several orders of magnitude larger than that of the APC (black line) in the relative wide energy range, *i.e.* from -0.4 eV to 0.4 eV. At the Fermi level, the transmission coefficients of the PC and APC are predicted to be 0.04 and 1.18×10^{-7}, respectively. This remarkable transmission coefficient difference between the PC and APC results in a huge TMR ratio of $3.08\times10^{7}\%$, according to Eq.(2). It should be pointed out that this TMR ratio is generally larger than the experimental results for the similar junctions [17, 26]. One most possible reason is that in experiments the existence of defects (*i.e.* oxygen vacancy, substituting, and doping) cannot be avoided, which affects the performance of the MTJ. For example, the introduction of oxygen vacancies destroys the half-metallicity of HMFs, then reduces spin injection efficiency [27, 39].

FIG. 2 (c) and (d) show the zero-bias transmission spectra of MTJ1 in the PC and APC, respectively, here, the red and black lines stand for the spin-up and spin-down electrons. Clearly, we observe a nearly perfect spin-filtering effect in MTJ1 with the PC. In the energy range from -0.3 eV to 0.5 eV, the spin-up transmission coefficients are significantly larger than that of the spin-down electrons. At the Fermi level, the transmission coefficient for the spin-down electrons is close to zero, *i.e.* less than 10^{-8}, while for the spin-up channel, the transmission coefficient is about 0.04. That is to say, the spin transport properties of MTJ1 is dominated by the spin-up electrons. This low-bias transport properties governed by the spin-up electrons have been observed in various MTJs, *i.e.* MgO barrier-based MTJs and half-metal electrodes-based MTJs [7, 11]. As for MTJ1 in the APC, the shapes of the spin-up transmission spectra almost coincides with that of the spin-down electrons. The transmission coefficient of the spin-down electrons is about 5.89×10^{-8} at the Fermi level, which

DOI:10.1063/1674-0068/cjcp2009170 ©2021 Chinese Physical Society

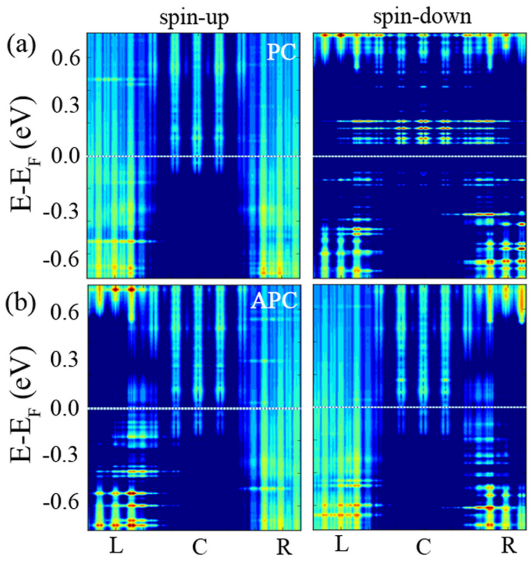

FIG. 3 Spin-resolved projected DOS of MTJ1 in (a) PC and (b) APC along the transport direction, here, left and right panels stand for the spin-up and spin-down electrons, respectively, and the white dashed line labels for the Fermi level for clarity.

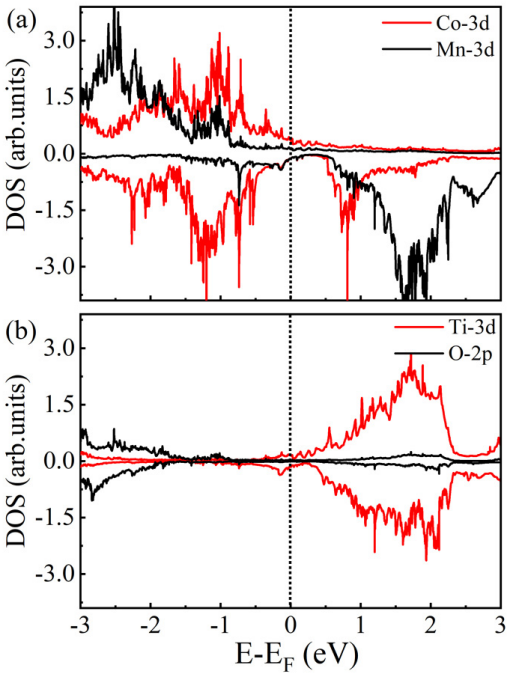

FIG. 4 (a) For MTJ1 in the PC, partial DOS of Co 3d and Mn 3d orbitals at the MnSi-TiO_2 interface, labeled with the red and black lines, respectively. (b) Partial DOS of Ti 3d (red line) and O 2p (black line) orbitals.

is significantly less than that of the spin-up electrons in the PC (0.04).

To explore the nature of the above dramatically different spin-dependent transport process in MTJ1 with two different magnetization configurations, we calculate the spin-resolved projected DOS along the transport direction, as shown in FIG. 3 (a) and (b) for the PC and APC, respectively. As for the PC case, the right and left electrodes have spin-up electronic states at the Fermi level, but for the spin-down electrons, no electronic states of two electrodes appear, due to the half-metallic nature of Heusler alloy Co_2MnSi electrode. Moreover, one can see that the Fermi level crosses spin-up electronic states of $SrTiO_3$ barrier layer. These observations show that the transport process is dominated by the spin-up electrons, meaning that the spin injection efficiency is close to 100%. In FIG. 3(b), for the APC, there are several spin-up and spin-down electronic states at the Fermi level, note that, the spin-down electronic states appear in the left electrode, which provides the spin-down electrons, but there are not spin-down electronic states in the right electrode, which can receive the spin-down electrons from the left electrode. At the same time, the left electrode cannot provide the spin-up electrons for the right electrode to receive. So, the asymmetry distribution of the PDOS of the left and right electrodes, as shown in FIG. 3(b), hinders the electron transport, which results in the transmission coefficient in the APC being significant less than that in the PC, as shown in FIG. 2(b), then a huge TMR appears.

Previous experimental and theoretical investigations have shown that the spin transport properties of MTJ strongly depend on the local geometric distortion and electronic structures of the interface between electrode and barrier layer [40, 41], one needs to see the local geometries and electronic structures at the MnSi-TiO_2 interface in MTJ1 in more detail. Here, taking MTJ1 in the PC as an example, we calculate the partial DOS of Co 3d (red line) and Mn 3d (black line) orbitals in the MnSi-TiO_2 interface, labeled with a circle in FIG. 2(a), and the partial DOS of Ti 3d (red line) and O 2p (black line) orbitals, and plot them in FIG. 4 (a) and (b), respectively. At the interface region, the Co−Si bonds are compressed by 0.13 Å, and the lengths of Ti−O, Ti−Sr, Mn−Si and Mn−Co bonds are elongated by 0.13, 0.04, 0.17, and 0.25 Å, respectively, compared to the corresponding bond lengths in bulk Co_2MnSi and $SrTiO_3$. It is clear that the interfacial electronic states are obviously modified due to the interface local structural relax. We observe a relative small decrease of the partial DOS of Co 3d orbital. The spin-up occupied elec-

DOI:10.1063/1674-0068/cjcp2009170 ©2021 Chinese Physical Society

tronic states and the spin-down conduction bands of Mn 3d orbital shift to lower energy. Due to the charge transfer (about 0.75 e) from two Co_2MnSi electrodes to $SrTiO_3$ barrier layer through the interface, the magnetic moment of Mn atoms increases by 1.1 μ_B and the nonmagnetic Ti atoms in $SrTiO_3$ bulk become magnetic in the interface (the Ti atomic moment magnetic moment is about 0.1 μ_B), and then the partial DOS of Ti 3d orbital are obviously spin-polarized, which plays an important role in spintronics applications. Most of these theoretical results for describing the MnSi-TiO_2 interface agree well with previous reports [28, 30].

FIG. 5 (a) and (b) illustrate the in-plane wave vector $k_{||}$ dependence transmission of MTJ1 in the PC at the Fermi level for the spin-up and spin-down electrons, respectively. Clearly, a broad peak is observed locating around $k_{||}$=(0, 0), as shown in FIG. 5(a), indicating that the $k_{||}$ dependence of MTJ1 conductance of the spin-up channel originates from the coherent tunneling. In contrast, for the spin-down electrons, there is no peak at $k_{||}$=(0, 0), while some spiky peaks appear, as shown in FIG. 5(b), and the corresponding transmission coefficients are very small. The average transmission coefficients over the Brillouin zone of the spin-up and spin-down electrons are about 0.04 and 5.37×10^{-12}, respectively. This observation again verifies that the transport behavior of MTJ1 in the PC is governed by the spin-up electrons, consisting with the results shown in FIG. 2(c).

Previous investigations have reported that the TMR of MTJ depends on the barrier thickness [7, 42]. Here, we tune the thickness of $SrTiO_3$ barrier layer in MTJ1, and the obtain results are similar to those plotted in FIG. 2(b)−(d). Note that, the value of the TMR ratio is changed to be (2.82×10^7)% and (2.66×10^6)% for the 7 and 15 atomic barrier layers, respectively. That is to say, the huge TMR oscillates as a function of tuned barrier thickness. Similar oscillated TMR behavior has been experimentally observed in Fe/MgO/Fe TMJ [6], which implies that the huge TMR is coherent spin-polarized tunneling in MTJ1, and the $SrTiO_3$ barrier layer plays a selective filtration role in transport.

Finally, the calculated zero-bias transmission spectra of MTJ2, MTJ3 and MTJ4 are presented in FIG. 6, here, the red and black lines stand for the transmission spectra for the PC and APC, respectively. It is clear that the spin-dependent transport properties of $Co_2MnSi/SrTiO_3/Co_2MnSi$ MTJs are sensitive to

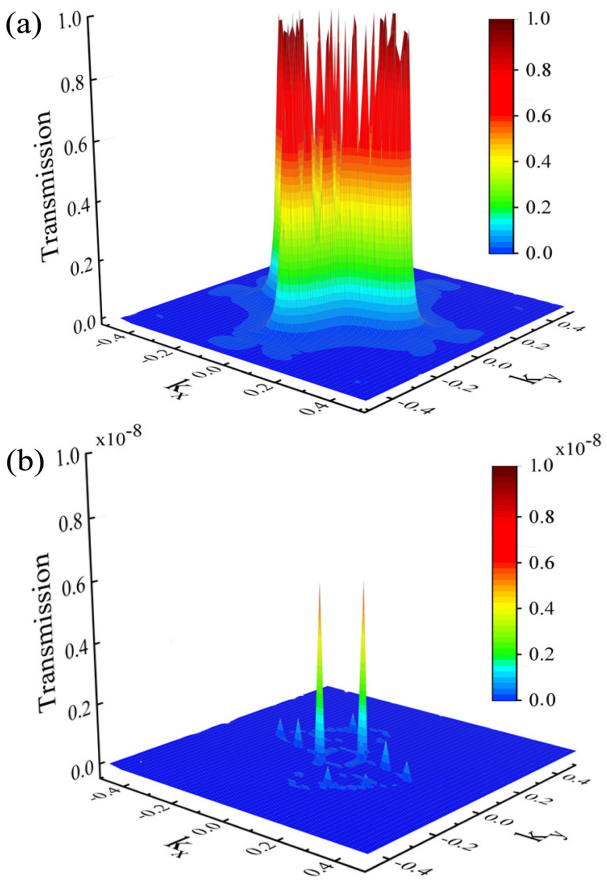

FIG. 5 In-plane wave vector $k_{||}$=(k_x, k_y) dependence of the spin-up (a) and spin-down (b) transmission of MTJ1 in the PC at the Fermi level.

TABLE I Calculated interfacial energies (E_{int}) and the interfacial distance (d_{int}) for four examined MTJs.

Structure	Interface	E_{int}/(eV/nm^2)	d_{int}/Å
MTJ1	MnSi-TiO_2	−78.94	1.8
MTJ2	MnSi-SrO	−76.90	2.0
MTJ3	Co_2-SrO	−70.00	2.6
MTJ4	Co_2-TiO_2	−77.20	1.9

the interface between electrode and barrier layer. At the Fermi level, the transmission coefficients for MTJ2, MTJ3, and MTJ4 in the PC are about 1.77×10^{-2}, 4.70×10^{-5}, 1.42×10^{-3}, while they are 1.02×10^{-8}, 3.90×10^{-8}, 8.14×10^{-11} for the APC case, respectively. It is clear that the values of these transmission coefficients depend mainly on the vertical distance at the MnSi-SrO, Co_2-SrO, and Co_2-TiO_2 interfaces of 2.0, 2.6, and 1.9 Å (summarized in Table I), respectively. Namely, a larger vertical distance results in a less transmission coefficient. Then, the corresponding TMR ratio

DOI:10.1063/1674-0068/cjcp2009170 ©2021 Chinese Physical Society

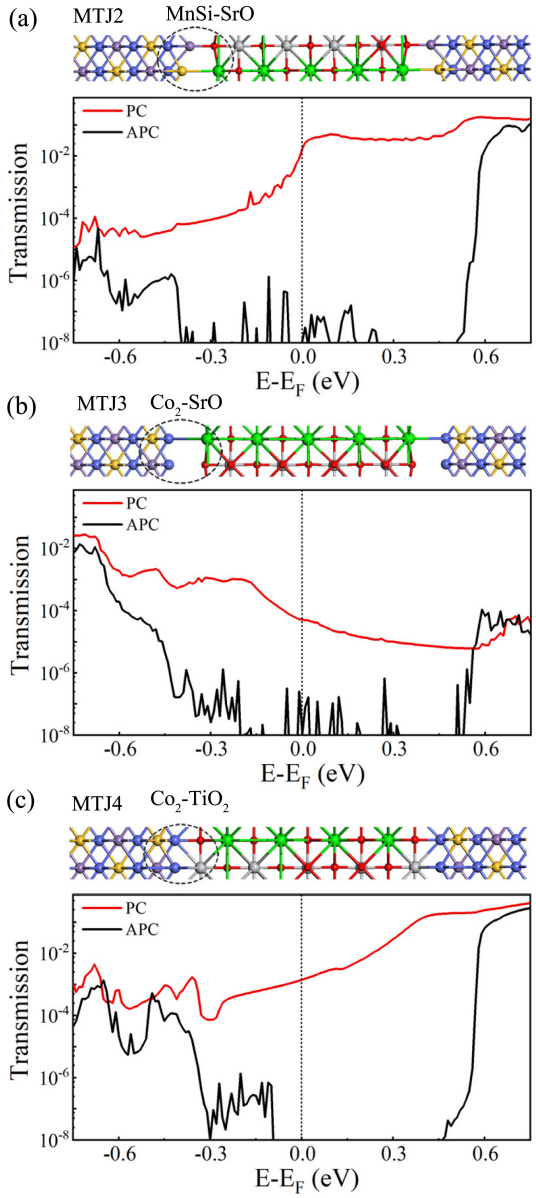

FIG. 6 Zero-bias transmission spectra of (a) MTJ2, (b) MTJ3, and (c) MTJ4 in the PC and APC, which are labeled with the red and black lines, respectively. Here, the top panel illustrates the corresponding scattering region of three MTJs.

is easily calculated to be $(3.43\times10^7)\%$, $(9.57\times10^4)\%$, and $(1.31\times10^7)\%$ for MTJ2, MTJ3, and MTJ4. It should be pointed out that these huge TMR ratios are theoretically predicted for $Co_2MnSi/SrTiO_3/Co_2MnSi$ MTJs with ideal single crystal structures, meaning that, to obtain high magnetoresistance, one has to improve the single crystal quality of Heusler alloy Co_2MnSi and $SrTiO_3$ barrier layer in experiments.

IV. CONCLUSION

In summary, we explore the spin-dependent transport properties of $Co_2MnSi/SrTiO_3/Co_2MnSi$ MTJs with four different interfaces via performing extensive DFT calculations within the NEGF technique. We find that the transport properties of $Co_2MnSi/SrTiO_3/Co_2MnSi$ MTJ strongly depend on the interface between Heusler alloy Co_2MnSi electrode and $SrTiO_3$ barrier layer. The transmission coefficient of MTJs with the MnSi-TiO_2 interface in the PC at the Fermi level is several orders of magnitude larger than that of in the APC, which results in a huge TMR. According to the calculated projected DOS of the MTJ1, the partial atomic DOS at the interface, and the in-plane wave vector dependence of transmission, we conclude that the predicted huge TMR originates from the coherent spin-polarized tunneling, due to the half-metallic nature of Co_2MnSi electrode and the significant spin-polarization of the interfacial metal atomic orbitals. These theoretical findings suggest that $Co_2MnSi/SrTiO_3/Co_2MnSi$ MTJs hold great potential in spintronics if one can improve the single crystal quality of Heusler alloy Co_2MnSi and $SrTiO_3$ barrier layer in experiments.

V. ACKNOWLEDGMENTS

This work was partially supported by the National Natural Science Foundation of China (No.21873088 and No.11634011) and the Natural Science Foundation of the Anhui Higher Education Institutions (No.KJ2010A061 and No.KJ2016A144). Computational resources have been provided by CAS, Shanghai and USTC Supercomputer Centers.

[1] Y. Goto, T. Yanase, T. Shimada, M. Shirai, and T. Nagahama, AIP Adv. **9**, 085322 (2019).
[2] N. Kudo, M. Oogane, M. Tsunoda, and Y. Ando, AIP Adv. **9**, 125036 (2019).
[3] L. Lang, Y. Jiang, F. Lu, C. Wang, Y. Chen, A. D. Kent, and L. Ye, Appl. Phys. Lett. **116**, 022409 (2020).
[4] I. I. Oleinik, E. Y. Tsymbal, and D. G. Pettifor, Phys. Rev. B **62**, 3952 (2000).
[5] W. H. Butler, X. G. Zhang, T. C. Schulthess, and J. MacLaren, Phys. Rev. B **63**, 054416 (2001).
[6] S. Yuasa, T. Nagahama, A. Fukushima, Y. Suzuki, and K. Ando, Nat. Mater. **3**, 868 (2004).
[7] D. Waldron, V. Timoshevskii, Y. Hu, K. Xia, and H. Guo, Phys. Rev. Lett. **97**, 226802 (2006).

DOI:10.1063/1674-0068/cjcp2009170 ©2021 Chinese Physical Society

[8] S. Ikeda, K. Miura, H. Yamamoto, K. Mizunuma, H. D. Gan, M. Endo, S. Kanai, J. Hayakawa, F. Matsukura, and H. Ohno, Nat. Mater. **9**, 721 (2010).
[9] S. Kanai, F. Matsukura, and H. Ohno, Appl. Phys. Lett. **108**, 192406 (2016).
[10] M. Goto, Y. Wakatake, U. K. Oji, S. Miwa, N. Strelkov, B. Dieny, H. Kubota, K. Yakushiji, A. Fukushima, S. Yuasa, and Y. Suzuki, Nat. Nanotech. **14**, 40 (2019).
[11] M. Sun, X. Wang, and W. Mi, J. Phys. Chem. C **122**, 3115 (2018).
[12] X. Han, W. Mi, and X. Wang, J. Mater. Chem. C **7**, 4079 (2019).
[13] A. M. Bratkovsky, Phys. Rev. B **56**, 2344 (1997).
[14] J. D. Burton and E. Y. Tsymbal, Phys. Rev. B **93**, 024419 (2016).
[15] J. Han, J. Shen, and G. Gao, RSC Adv. **9**, 3550 (2019).
[16] M. I. Katsnelson, V. Y. Irkhin, L. Chioncel, A. I. Lichtenstein, and R. A. de Groot, Rev. Mod. Phys. **80**, 315 (2008).
[17] M. Bowen, M. Bibes, A. Barthélémy, J. P. Contour, A. Anane, Y. Lemaître, and A. Fert, Appl. Phys. Lett. **82**, 233 (2003).
[18] B. Hu, K. Moges, Y. Honda, H. X. Liu, T. Uemura, and M. Yamamoto, Phys. Rev. B **94**, 094428 (2016).
[19] A. Boehnke, U. Martens, C. Sterwerf, A. Niesen, T. Huebner, M. von der Ehe, M. Meinert, T. Kuschel, A. Thomas, C. Heiliger, and M. Münzenberg, Nat. Commun. **8**, 1 (2017).
[20] W. Rotjanapittayakul, J. Prasongkit, I. Rungger, S. Sanvito, W. Pijitrojana, and T. Archer, Phys. Rev. B **98**, 054425 (2018).
[21] H. C. Kandpal, G. H. Fecher, C. Felser, and G. Schönhense, Phys. Rev. B **73**, 094422 (2006).
[22] H. Kubota, J. Nakata, M. Oogane, Y. Ando, A. Sakuma, and T. Miyazaki, Jpn. J. Appl. Phys. **43**, L984 (2004).
[23] Y. Sakuraba, M. Hattori, M. Oogane, Y. Ando, H. Kato, A. Sakuma, T. Miyazaki, and H. Kubota, Appl. Phys. Lett. **88**, 192508 (2006).
[24] N. Tezuka, N. Ikeda, S. Sugimoto, and K. Inomata, Jpn. J. Appl. Phys. **46**, L454 (2007).
[25] E. Ozawa, S. Tsunegi, M. Oogane, H. Naganuma, and Y. Ando, J. Phys.: Conf. Ser. **266**, 012104 (2011).
[26] H. Liu, Y. Honda, T. Taira, K. I. Matsuda, M. Arita, T. Uemura, and M. Yamamoto, Appl. Phys. Lett. **101**, 132418 (2012).
[27] P. K. Rout, H. Pandey, L. Wu, Anupam, P. C. Joshi, Z. Hossain, Y. Zhu, and R. C. Budhani, Phys. Rev. B **89**, 020401(R) (2014).
[28] S. Nazir and U. Schwingenschlögl, Phys. Status Solidi RRL **10**, 540 (2016).
[29] J. Schmalhorst, A. Thomas, S. Kämmerer, O. Schebaum, D. Ebke, M. D. Sacher, and G. Reiss, Phys. Rev. B **75**, 014403 (2007).
[30] Y. Miura, H. Uchida, Y. Oba, K. Abe, and M. Shirai, Phys. Rev. B **78**, 064416 (2008).
[31] J. P. Perdew, K. Burke, and M. Ernzerhof, Phys. Rev. Lett. **77**, 3865 (1996).
[32] G. Kresse and J. Furthmüller, Phys. Rev. B **54**, 11169 (1996).
[33] G. Kresse and J. Furthmüller, Comput. Mater. Sci. **6**, 15 (1996).
[34] J. Taylor, H. Guo, and J. Wang, Phys. Rev. B **63**, 245407 (2001).
[35] M. Brandbyge, J. L. Mozos, P. Ordejón, J. Taylor, and K. Stokbro, Phys. Rev. B **65**, 165401 (2002).
[36] M. P. Raphael, B. Ravel, Q. Huang, M. A. Willard, S. F. Cheng, B. N. Das, R. M. Stroud, K. M. Bussmann, J. H. Claassen, and V. G. Harris1, Phys. Rev. B **66**, 104429 (2002).
[37] S. Picozzi, A. Continenza, and A. J. Freeman, Phys. Rev. B **66**, 094421 (2002).
[38] S. Piskunov, E. Heifets, R. I. Eglitis, and G. Borstel, Comput. Mater. Sci. **29**, 165 (2004).
[39] Y. Ke, K. Xia, and H. Guo, Phys. Rev. Lett. **105**, 236801 (2010).
[40] L. Shen, T. Zhou, Z. Bai, M. Zeng, J. Q. Goh, Z. M. Yuan, G. Han, B. Liu, and Y. P. Feng, Phys. Rev. B **85**, 064105 (2012).
[41] M. Stamenova, R. Mohebbi, J. Seyed-Yazdi, I. Rungger, and S. Sanvito, Phys. Rev. B **95**, 060403 (2017).
[42] M. Ansarino, H. M. Moghaddam, and A. Bahari, Physica E **107**, 80 (2019).

DOI:10.1063/1674-0068/cjcp2009170 ©2021 Chinese Physical Society